COMMUNICATION

3D Bioprinting of Vascularized, Heterogeneous Cell-Laden Tissue Constructs

*David B. Kolesky, Ryan L. Truby, A. Sydney Gladman, Travis A. Busbee, Kimberly A. Homan, and Jennifer A. Lewis**

The ability to create 3D vascularized tissues on demand would enable scientific and technological advances in tissue engineering,[1] drug screening,[2] and organ repair.[3–5] To produce 3D engineered tissue constructs that mimic natural tissues and, ultimately, organs, several key components – cells, extracellular matrix (ECM), and vasculature – need to be patterned in precise geometries. Each of these components plays a vital role in imparting, supporting, or sustaining the biomimetic function of the engineered tissue construct, respectively. Perhaps the most important of these components is the vasculature; without proximity to a perfused microvasculature that provides efficient nutrient, growth/signaling factor, and waste transport, most cells within bulk tissue constructs will not remain viable.[6,7] In fact, 3D engineered tissue constructs quickly develop necrotic regions without perfusable vasculature within a few hundred microns of each cell.[8,9] Unfortunately, the inability to create vascular networks within engineered tissue constructs has hindered progress in the field of tissue engineering for decades.

One emerging strategy for creating engineered tissue constructs is 3D printing.[10] To date, this technique has been primarily used to create acellular 3D scaffolds and molds,[11–14] which must be seeded with cells post-fabrication. Building tissue constructs by directly depositing cells or cell aggregates, known as bioprinting, has also recently been reported.[5,15,16] However, neither approach is currently capable of directly embedding vasculature, which severely constrains the overall dimensions of tissue constructs produced by these strategies. As an important step forward, researchers have introduced vascular channels by printing sacrificial carbohydrate glass filaments at temperatures above 100 °C, which are then encapsulated within cell-laden hydrogels via a molding process.[17] While elegant, this hybrid printing/molding technique is relegated to constructing simple tissue architectures composed of homogeneous cell-laden matrices. Yet, natural tissues are structurally complex and composed of multiple cell types.

Here, we report a new 3D bioprinting method for fabricating engineered tissue constructs replete with vasculature, multiple types of cells, and ECM. Creating these intricate, heterogeneous structures requires the ability to precisely co-print multiple materials in 3D (**Scheme** 1). Hence, we first implemented a custom-designed, large-area 3D bioprinter with four independently controlled printheads (Figure S1, Supporting Information). An initial demonstration of our multimaterial printing capability is provided in Figure S2 and Movie 1 in the Supporting Information. Four inks, each composed of poly(dimethyl siloxane) (PDMS) dyed with different fluorophores, are co-printed in a predefined sequence to produce a heterogeneous 3D architecture in which each layer is composed of a different material. This PDMS ink not only serves as a good model system, it is also used to print high-aspect-ratio borders around the fabricated engineered tissue constructs described below (Movie 2 in the Supporting Information).

Next, building on our earlier work on printing 3D microfluidic devices,[18] and self-healing materials[19] with embedded vasculature, we designed fugitive and cell-laden hydrogel inks to meet several important criteria. First, the inks must be compatible with one another during printing under ambient conditions. Second, the patterned cells and surrounding ECM must not be damaged during printing or the fugitive ink removal procedure. Notably, sacrificial inks, such as sugar and wax, are not suitable: they either require elevated printing temperatures[17] or harsh solvents for removal,[18] and/or they lack biocompatibility. Third, the resulting vasculature must be perfusable. Finally, both printed cells and those introduced by perfusion must remain viable.

To fabricate embedded vasculature, we developed an aqueous fugitive ink composed of Pluronic F127 that can be easily printed and removed under mild conditions. We selected this triblock copolymer, in part because of its demonstrated effectiveness in printing synthetic microvascular networks.[19] More importantly, it is biologically inert to multiple cell types over the short time periods needed to complete the fabrication process. Pluronic F127 is composed of a hydrophobic poly(propylene oxide) (PPO) segment and two hydrophilic poly(ethylene oxide) (PEO) segments arranged in a PEO-PPO-PEO configuration (**Figure 1**a). This material undergoes thermally reversible gelation above a critical micelle concentration (CMC ≈ 21 wt%) and temperature, which decreases from approximately 10 °C to 4 °C as the PEO-PPO-PEO concentration increases above the CMC. When both of these critical parameters are exceeded, micelles form as the hydrophilic PEO segments self-assemble into corona that are well solvated by water, while the hydrophobic PPO segments tightly associate within the micelle cores.[20,21] However, below the gelation temperature, the hydrophobic PPO units are hydrated, such that individual PEO-PPO-PEO species become soluble in water giving rise to a gel-to-fluid transition for systems whose concentration exceeds the CMC. We exploit

D. B. Kolesky, R. L. Truby, A. S. Gladman, T. Busbee, Dr. K. A. Homan, Prof. J. A. Lewis
School of Engineering and Applied Sciences
Wyss Institute for Biologically Inspired Engineering
Harvard University
Cambridge, MA 02138, USA
E-mail: jalewis@seas.harvard.edu

DOI: 10.1002/adma.201305506

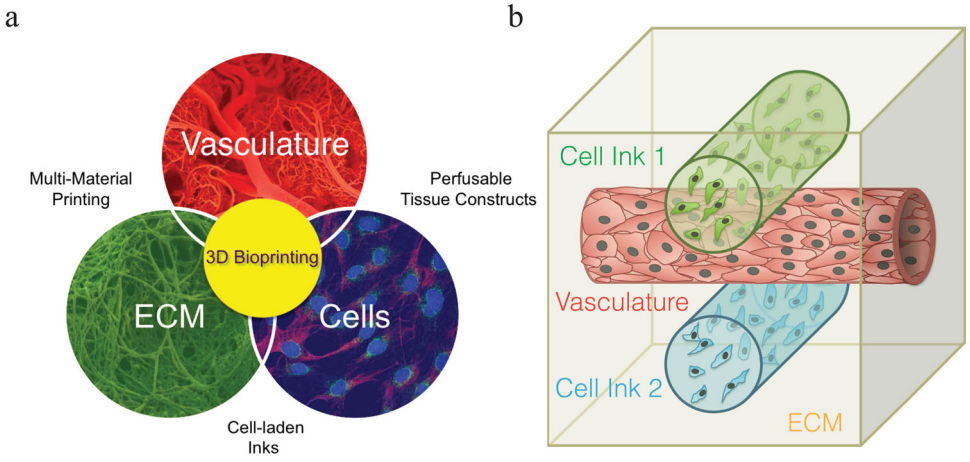

Scheme 1. Schematic views of our 3D bioprinting approach (left), in which vasculature, cells, and ECM are co-printed to yield engineered tissue constructs composed of heterogeneous subunits (right).

this behavior to produce a highly concentrated ink (40 wt% Pluronic F127) that exhibits a strong shear-thinning response when the applied shear stress exceeds the shear yield stress (τ_y) (e.g., during printing), as well as a plateau shear elastic modulus (G') that exceeds the shear loss modulus (G'') when the applied shear stress is below τ_y (e.g., after printing). We find that the ink elasticity is ca. 2×10^4 Pa at 22 °C. Below ca. 4 °C, the ink liquefies and its elasticity decreases by several orders of magnitude, thereby facilitating its removal from printed tissue constructs.

To create the ECM, we synthesized gelatin methacrylate (GelMA) for use as a bulk matrix and cell carrier. This material is selected due to its low-cost, abundance, ease of processing, and biocompatibility.[22] GelMA is denatured collagen that is modified with photopolymerizable methacrylate (MA) groups, allowing the matrix to be covalently cross-linked by UV light after printing. Physical gelation arises from the assembly of intermolecular triple helices that possess a structure similar to collagen [23] (Figure 1b). By varying the concentration, degree of methacrylation, and temperature, the shear yield stress and elastic modulus of aqueous GelMA systems can be systematically tuned.[22,24] We specifically produce a concentrated ECM-like ink by dissolving 15 wt/v% GelMA in cell culture media. Above approximately 23 °C, the ink is a low viscosity fluid with a G' value below 10^{-1} Pa. Upon cooling below 23 °C, the ink undergoes gelation yielding a clear, viscoelastic matrix material. The ink elasticity increases with decreasing temperature, with G' values of ca. 10^3 Pa and 2×10^4 Pa observed at 22 °C and 4 °C, which correspond to typical conditions for printing and fugitive ink removal, respectively.

We used the same aqueous GelMA system to create cell-laden inks for 3D bioprinting. Prior studies have shown that cells adhere, remodel, and migrate through GelMA due to the presence of integrin-binding motifs and matrix metalproteinase sensitive groups.[22,25] We find that the incorporation of a moderate concentration, 2×10^6 cells mL^{-1}, of fibroblast cells into the 15 wt/v% GelMA ink (Figure 1c) does not significantly alter the temperature at which gelation ensues or the ink elasticity over the temperature range of interest (i.e., 2 °C to 40 °C). Hence, both the pure and cell-laden GelMA inks can be printed and further processed, as needed, in the same manner.

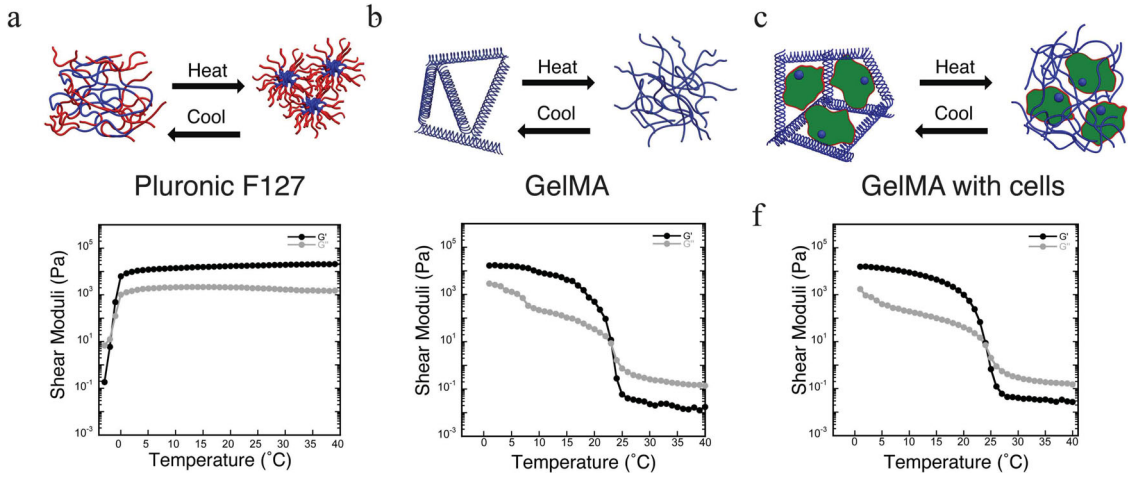

Figure 1. Schematic views of thermally reversible gelation and the corresponding shear elastic (G') and loss moduli (G'') measured as a function of temperature for: a) Pluronic F127 fugitive, b) pure GelMA, and c) 10T1/2 fibroblast-cell-laden GelMA inks.

ADVANCED MATERIALS
www.advmat.de

www.MaterialsViews.com

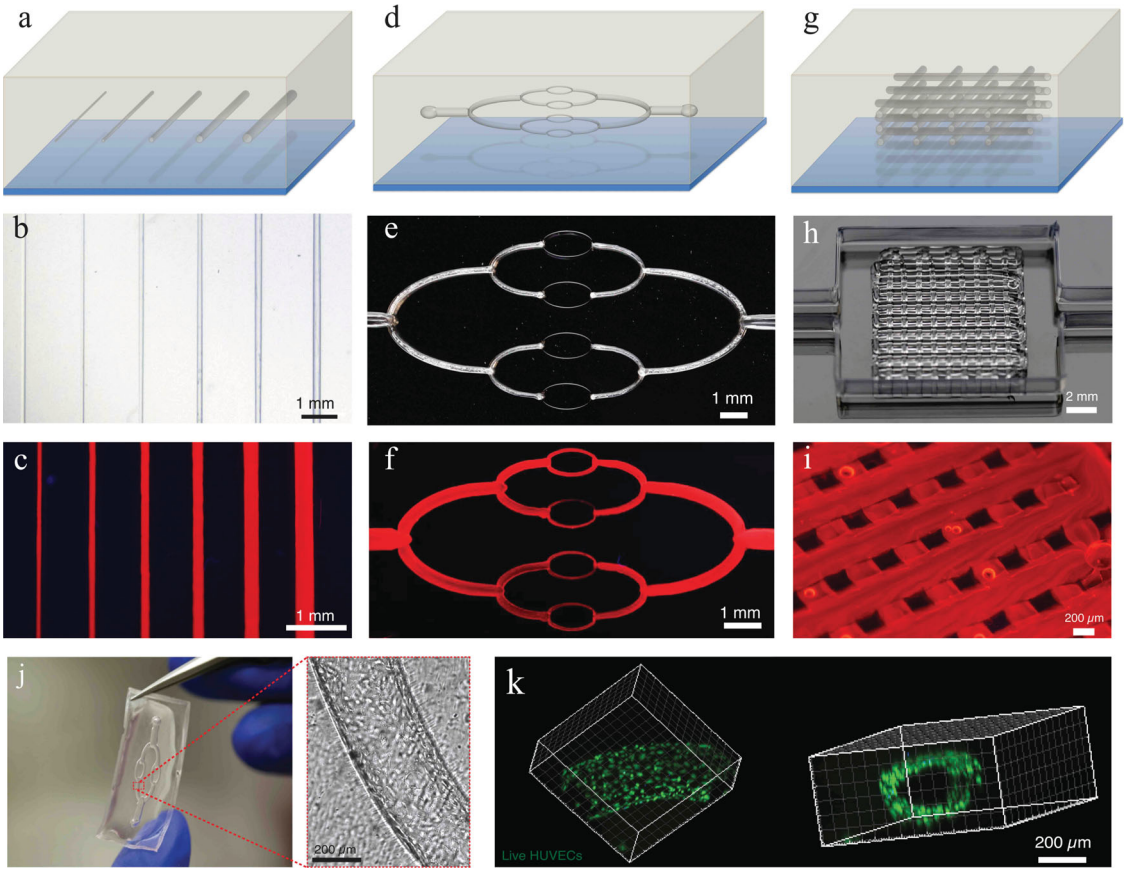

Figure 2. Schematic illustrations, optical images, and fluorescent images of 1D (Column 1: a–c), 2D (Column 2: d–f), and 3D (Column 3: g–i) embedded vascular networks that are printed, evacuated, and perfused with a water-soluble fluorescent dye. Bottom row: j) Optical image of representative microchannel within a 2D vascular network perfused with a HUVEC suspension and k) confocal image of live HUVEC cells lining the microchannel walls.

The differences in thermally reversible gelation observed for the fugitive Pluronic F127, pure GelMA, and cell-laden GelMA inks give rise to three distinct processing windows. Between approximately 4 °C and 22 °C, each ink is stiff and exhibits a solid-like response, where $G' > G''$. At $T \geq 22$ °C, the Pluronic F127 fugitive ink is stiff and solid-like ($G' > G''$), while the pure and cell-laden GelMA inks are liquids that flow readily. Below ca. 4 °C, the Pluronic F127 fugitive ink is a liquid that flows readily, while the pure and cell-laden GelMA inks are stiff and solid-like ($G' > G''$).

We take advantage of this complimentary behavior to print representative 1D, 2D, and 3D vascular networks, which are subsequently embedded in a pure GelMA matrix (i.e., acellular ECM). The schematic views and corresponding images of each printed vascular network design are shown in **Figure 2**. After introducing and photopolymerizing the GelMA matrix, the fugitive ink is removed by cooling the printed constructs below 4 °C yielding open channels (Figure S3, Supporting Information). After this process, representative vascular networks are injected with a fluorescent red dye to aid visualization. Within each construct, the diameter of printed filaments can be altered on demand by modifying the printing pressure, speed, or nozzle height. For example, we printed 1D microchannel arrays with diameters increasing from 45 μm to 500 μm using a single 30 μm nozzle and increasing the printing pressure and nozzle height in a stepwise fashion between each printed feature (Figure 2a–c). Cross-sectional images of these channels, shown in Figure S4 in the Supporting Information, reveal that their final diameters range from ca. 100 μm–1 mm. Since the GelMA ink has a higher water content than the fugitive ink, the printed vascular features swell as water diffuses into fugitive Pluronic F127 ink from the surrounding matrix. Indeed, we find that their channel diameters nearly double in size, with a swelling ratio that is independent of initial feature size for this ink combination.

The 2D vascular network design mimics the hierarchical, bifurcating motifs found in biological systems; large channels bifurcate to form smaller channels that maximize efficient blood flow, nutrient transport, and waste removal while minimizing the metabolic cost.[26] These 2D hierarchical vascular networks are printed using 30 μm nozzle (Figure 2d–f). The as-printed, largest channels (ca. 650 μm in diameter) provide a single inlet and outlet for perfusion, while the smallest channels (ca. 150 μm in diameter) reduce the characteristic diffusion distance between adjacent conduits. Finally, we printed the 3D microvascular network design shown in Figure 2g–i, which consists of a 3D periodic array of uniform microchannels. Because the embedded microchannels are interconnected in all three dimensions, the fugitive ink can be removed from the surrounding GelMA matrix quickly and with high fidelity (Supporting Information, Movie 3).

Engineered tissue constructs must be able to support the attachment and proliferation of endothelial cells, which line vascular walls providing a barrier to fluid diffusion, while simultaneously facilitating homeostatic functions[27] and helping establish vascular niches specific to various tissues.[28,29] To promote endothelialization, we injected representative 2D hierarchical bifurcating networks with a human umbilical vein endothelial cell (HUVEC) suspension followed by gentle rocking (Figure 2j). After 48 h, we find that these cells retained greater than 95% viability and assembled into a nearly confluent layer, as determined by live/dead staining coupled with confocal imaging within a representative, bifurcated microchannel (Figure 2k, Supporting Information, Movie 4). In a separate experiment, we directly injected animal blood into the inlet of the 2D vascular network and observed that it rapidly flowed through the entire network to outlet (Figure S5 and Movie 5 in the Supporting Information). To further demonstrate the versatility of our approach, we printed and encapsulated a 1D vascular network within another biologically relevant matrix (i.e., fibrin gel) and showed that HUVECs attach and proliferate in those channels as well (Figure S5 and Movie 6 in the Supporting Information). These initial demonstrations, while simple, illustrate the potential to create perfusable vasculature of nearly arbitrary design with dimensions akin to those found in natural tissues. While it is possible to print finer capillaries, those would ideally be generated via directed capillary growth (e.g., angiogenesis).[30,31] Efforts are now underway to determine the optimal way to combine 3D printing and biological self-assembly to produce fully vascularized, engineered tissue constructs.

To fabricate engineered tissue constructs replete with blood vessels, multiple types of cells, and ECM, we printed 3D heterogeneous structures of varying design. As indicated previously, the PDMS ink is first printed in the form of a high-aspect ratio border that surrounds each tissue construct. We initially fabricated the multilayer, tissue construct shown in **Figure 3** by co-printing two inks at 20–22 °C: the fugitive Pluronic F127 ink and a cell-laden GelMA ink that contains green fluorescent protein expressing human neonatal dermal fibroblasts (HNDFs) at a concentration of 2×10^6 cells mL^{-1} through 200 μm nozzles in a predefined sequential process. We then deposited pure GelMA ink at 37 °C to fully encapsulate the printed features, followed by photopolymerization to cross-link the GelMA matrix. Next, the fugitive ink is liquefied and removed from the 3D construct and the evacuated channels are endothelialized, as described above. Using confocal microscopy, we clearly observe both the green fluorescent protein expressing HNDFs in GelMA and the red-HUVECs that line the 3D vasculature embedded within this tissue construct.

To demonstrate patterning of multiple cell types, we printed an engineered tissue construct composed of semi-woven features printed in and out of plane (**Figure 4**, and Supporting Information, Movie 7). This 4-layer construct is produced in a layer-wise build sequence by co-printing four inks through 200 μm nozzles: PDMS, fugitive Pluronic F127 and two different cell-laden GelMA inks, followed by deposition of pure GelMA ink at 37 °C to fully encapsulate the printed features, and then photopolymerization to cross-link the GelMA matrix. The cell-laden GelMA inks contained either green fluorescent protein expressing HNDFs or non-fluorescent 10T1/2s, an established mouse fibroblast line at concentrations of 2×10^6 cells mL^{-1}. These cell types are used solely for demonstration purposes; in practice, human and animal cells would not be combined in engineered tissue constructs produced by our approach. Figure 4c shows an image of the 3D structure directly after printing. After fabrication, the fugitive ink is liquefied and removed from the 3D tissue construct. The evacuation procedure, which is identical to that used for each printed construct, involves placing empty syringe tips into the inlet and outlet microchannels and then aspirating the vascular network under a modest vacuum (Figure 4f, and Supporting Information, Movie 8). The removal process is rapid and yields a high fidelity, interpenetrating vasculature, which is then endothelialized and perfused with cell culture media. Using microscopy, we identified the locations of the three cell types that are independently stained: GFP HNDF (green), DAPI 10T1/2 (blue), and RFP HUVEC (red) cells. The semi-woven nature of this engineered tissue construct is clearly identifiable in the composite fluorescence microscopy image taken after 2 days of culture shown in Figure 4g.

As a final step, we investigated the viability of both the printed GFP HNDF cells and 10T1/2 fibroblast cells in GelMA over the course of 1 week. At day 0, the cell viability is 70% for the HNDFs and 61% for 10T/12 cells; however, these values increased to 81% and 82%, respectively, after 7 days (Figure 4h). While we find that the initial cell viability is lower compared to the control, the printed cells proliferate over time leading to similar levels of cell viability after 1 week in culture (Figure S6, Supporting Information). These observations suggest that our

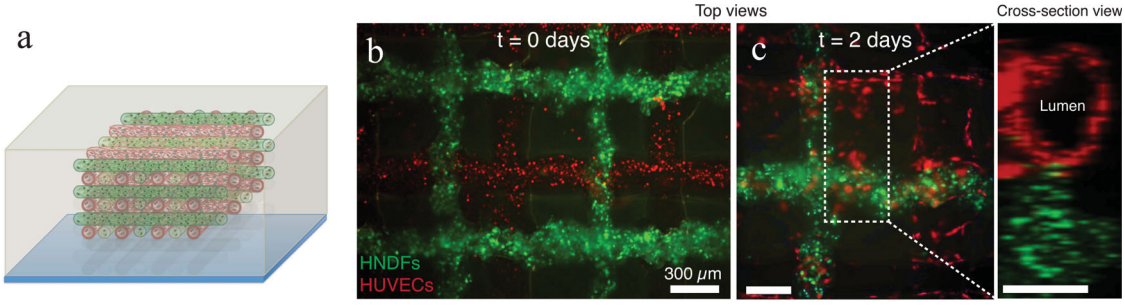

Figure 3. a–c) Schematic view (a) and fluorescence images (b,c) of an engineered tissue construct cultured for 0 and 2 days, respectively, in which red and green filaments correspond to channels lined with RFP HUVECs and GFP HNDF-laden GelMA ink respectively. The cross-sectional view in (c) shows that endothelial cells line the lumens within the embedded 3D microvascular network.

ADVANCED MATERIALS
www.advmat.de

www.MaterialsViews.com

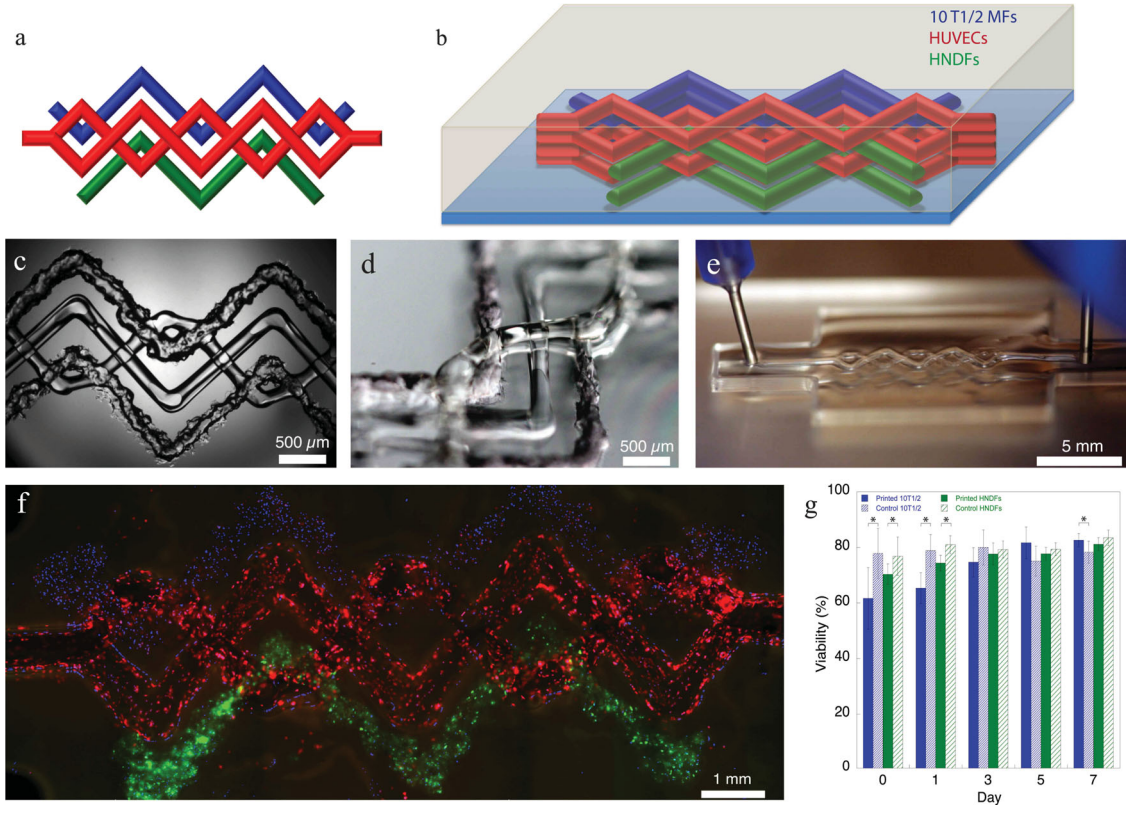

Figure 4. a,b) Schematic views of the top-down and side views of a heterogeneous engineered tissue construct, in which blue, red, and green filaments correspond to printed 10T1/2 fibroblast-laden GelMA, fugitive, and GFP HNDF-laden GelMA, inks, respectively. The gray shaded region corresponds to pure GelMA matrix that encapsulates the 3D printed tissue construct. Note: The red filaments are evacuated to create open microchannels, which are endothelialized with RFP HUVECs. c) Bright field microscopy image of the 3D printed tissue construct, which is overlayed with the green fluorescent channel. d) Image showing the spanning and out-of-plane nature of the 3D printed construct. e) Image acquired during fugitive ink evacuation. f) Composite image (top view) of the 3D printed tissue construct acquired using three fluorescent channels: 10T1/2 fibroblasts (blue), HNDFs (green), HUVECs (red). g) Cell-viability assay results of printed 10T ½ fibroblast-laden and HNDF-laden GelMA features compared to a control sample (200–300 μm thick) of identical composition. The asterisks indicate differences with $p < 0.05$ obtained from student's *t*-test.

3D bioprinting approach is non-destructive to both primary human fibroblasts and an immortalized mouse fibroblast line. The decreased initial viability may arise from the shear or extensional stress that the cells experience during the printing process.[32] Others have reported that the applied pressure, nozzle diameter, cell type, and environmental conditions influence cell viability after printing.[33,34] Another important parameter is the total build time required to fabricate the desired engineered tissue construct. We anticipate that there is a maximum time over which these cell-laden inks can be stored in the ink reservoir prior to being harmed. To fully optimize this approach, we plan to systematically study each of these important parameters in future experiments. By implementing multinozzle printheads,[35] which we designed previously for high-throughput, multimaterial printing, the characteristic build times would be vastly reduced. For example, it would require 3 days to print an engineered tissue construct with a volume of ca. 1000 cm^3, comparable to a typical adult human liver, using a single (200 μm) nozzle at typical printing speeds. However, this same volume could be printed in 1 h using a 64-multinozzle array. The scalable nature of our approach is also relevant for applications such as drug screening, in which arrays of 3D tissues constructs could be printed in parallel within standard well plates (Figure S7, Supporting Information).

In summary, we report a new approach for creating vascularized, heterogeneous tissue constructs on demand based on 3D bioprinting. This highly scalable platform allows one to produce engineered tissue constructs in which vasculature and multiple cell types are programmably placed within extracellular matrices. These 3D microengineered environments open new avenues for drug screening and fundamental studies of wound healing, angiogenesis, and stem cell niches. With further refinement, our technique may lead to the rapid manufacturing of functional 3D tissues and, ultimately, perhaps organs.

Experimental Methods

Ink Formulations: We created several inks for 3D printing of engineered tissue constructs. The first ink was composed of a two-part silicone elastomer (SE 1700, DOW Chemical) with a 10:1 base to catalyst (by weight) that is homogenized using a mixer (AE-310, Thinky Corp, Japan) and subsequently loaded into a syringe (EFD Inc., East Providence, RI, USA) at room temperature and centrifuged to remove any air bubbles. This ink is dyed with different fluorophores (Risk Reactor Inc., Santa

Ana, CA, USA) to demonstrate multimaterial printing. This ink is also used to print a border region composed of high-aspect ratio walls around each tissue construct.

The second ink was composed of 40 wt% Pluronic F127 (Sigma) in deionized, ultrafiltrated (DIUF) water. The ink is homogenized using a Thinky mixer until the powder was fully dissolved, and subsequently stored at 4 °C. Prior to use, the ink is loaded in a syringe (EFD Inc., East Providence, RI, USA) at 4 °C and centrifuged to remove any air bubbles. This ink was used to print 1D, 2D, and 3D vascular networks.

The final inks were composed of pure or cell-laden GelMA solutions. We synthesized GelMA following a modified procedure, reported previously.[22] First, a 10w/v% gelatin solution was prepared by dissolving gelatin (Type A, 300 bloom from porcine skin, Sigma) in Dulbelco's phosphate buffered saline (DPBS) warmed to 60 °C for 2 h under vigorous stirring. The solution temperature was maintained between 60 °C and 70 °C during gelatin dissolution, after which it was lowered to 50 °C. To produce GelMA with a 50% degree of methacrylation,[22] 0.14 mL of methacrylic anhydride (Sigma) was then added drop-wise to the gelatin solution for each gram of gelatin in solution. The gelatin methacrylation reaction was allowed to proceed for 4 h at 50 °C under vigorous stirring. The methacrylation reaction was then quenched by dilution of the reaction solution with DPBS warmed to 40 °C to yield a GelMA concentration of 4.5 w/v%. To remove excess methacrylic acid and methacrylic anhydride, GelMA was precipitated overnight by the addition of ice-cold acetone to the reacted solution at a 1:4 ratio of GelMA to acetone. Acetone was then decanted from the precipitated GelMA, and the precipitate was dried under flowing air for 30 min before being dissolved in 10 w/v% in DPBS warmed to 40 °C. This warm GelMA solution is vacuum filtered through a 0.2 μm filter (Corning Bottle-Top Vacuum Filtration System), transferred to a 12–14 kDa molecular weight cutoff (MWCO) dialysis tubing, and dialyzed against deionized (DI) water for 3 days (the dialysis media was changed twice daily) to remove any remaining methacrylic acid and salts from the DPBS. Lastly, the GelMA was frozen overnight at −80 °C, lyophilized for four days, and stored at −20 °C.

Pure GelMA inks were prepared by first dissolving GelMA powder in warm 1:1 DMEM:EGM-2 cell-culture media at 15 wt/v%. Irgacure 2959 (BASF) was added to the solution at 0.3 wt% as a photoinitiator, the solution was briefly vortex mixed, and stored at 37 °C until fully dissolved. Once dissolved, the solution was centrifuged to remove air bubbles. Unused GelMa solution was stored in dark conditions at 2–8 °C to prevent unintentional crosslinking via ambient light.

Cell-laden GelMA inks were created by first removing 10 T1/2 or HNDFs from culture flasks via the standard trypsinization technique. The cells were then dispersed in 15 wt% GelMA/media solutions at 2×10^6 cells mL^{-1}. The cell-laden ink was pipetted up and down to mix thoroughly. Each GelMA-based ink was then loaded into a syringe at 37 °C and allowed to cool to room temperature (ca. 22 °C) for 15 min prior to use.

Rheological Characterization: The ink rheology was measured using a controlled stress rheometer (DHR-3, TA Instruments, New Castle, DE, USA) with a 40 mm diameter, 2° cone and plate geometry. The shear storage (G') and loss (G'') moduli were measured at a frequency of 1 Hz and an oscillatory strain of 0.01. Temperature sweeps are performed using a peltier plate over the range from −5 °C to 40 °C. Samples were equilibrated for 5 min before testing and for 1 min at each subsequent temperature to minimize thermal gradients throughout the sample.

Cell Culture and Maintenance: C3H/10T1/2, Clone 8 cells (ATCC CCL-226TM) and green fluorescent protein-expressing human neonatal dermal fibroblast cells (GFP-HNDFs, Angio-Proteomie) were maintained in Dulbelco's modified Eagle medium containing high glucose and sodium pyruvate (DMEM) (GlutaMAXTM, Gibco) and supplemented with 10% fetal bovine serum (FBS) (Gemini Bio-Products). Primary human umbilical vein endothelial cells (HUVECs) (Lonza) and red fluorescent protein-expressing HUVECs (RFP-HUVECs) (Angio-Proteomie) were maintained in EMG-2 media (complete EGMTM-2 BulletKitTM, Lonza). All the cell cultures were passaged per the respective vendor's instructions. HUVECs, GFP-HNDFs, and RFP-HUVECs were not used beyond the ninth passage.

Glass-Slide Treatment: The engineered tissue constructs were printed onto a glass slide that have been pre-treated to promote bonding of GelMA-based inks. The glass slides were first cleaned via sonication in a series of solvents (isopropyl alcohol, ethanol, and deionized water) and subsequently air-dried. The slides are then soaked in a 5% 3-(trimethoxysilyl)propyl methacrylate (Sigma) in toluene solution at 60 °C overnight, rinsed with isopropyl alcohol, and air-dried prior to their use as substrates.

Multi-Material 3D Bioprinting: All the fabricated 3D structures were printed using a custom-built 3D printer with an overall build volume of 725 mm × 650 mm × 150 mm (ABG 10000, Aerotech Inc., Pittsburgh, PA, USA) equipped with four independent, z-axis-controlled ink reservoirs. Inks were housed in separate syringe barrels, and nozzles of varying size were attached via a luer-lok. Several types of nozzles were used, including borosilicate (30 μm in diameter produced using a P-2000 micropipette puller, Sutter Instrument Co., Novato, CA , USA) stainless steel (100 μm or 410 μm in diameter), and tapered plastic (200 μm in diameter) nozzles (EFD Inc., East Providence, RI, USA). Each ink was extrusion printed through the nozzle orifice under an applied air pressure (800 Ultra dispensing system, EFD Inc., East Providence, RI, USA) at speeds of 1–10 mm s^{-1} and pressures ranging from 20–60 psi. Before printing, the nozzles are aligned using orthogonally mounted optical micrometers (LS-7600 series, Keyence, Japan) to determine their respective X–Y offsets. The cell-laden inks are printed up to maximum of 2 h after mounting to limit cell damage due to lack of oxygen.

Engineered tissue constructs were produced by sequentially co-printing multiple inks. First, a border was printed by depositing the PDMS ink through a 200 μm tapered nozzle. A thin layer of the GelMA matrix was then deposited into bordered region at 37 °C. This layer was then cooled to 15 °C to induce rapid gelation. Next, the fugitive Pluronic F127 and cell-based GelMA inks were printed directly onto GelMA-coated or bare glass surfaces. After printing, the patterned vascular and cell-laden features were encapsulated by depositing a pure GelMA ink heated to 37 °C. The entire structure was illuminated with UV light source (Omnicure EXFO, 5 mW cm^{-2} for 60 s) to crosslink the GelMA species within the bulk matrix as well as cell-laden, patterned features. The entire structure is then cooled to 4 °C to liquefy the printed Pluronic F127 features. Two empty syringes outfitted with 200 μm diameter stainless-steel nozzles are then inserted through the printed construct into the liquefied regions. A modest vacuum is applied to remove the Pluronic F127 ink from those regions, leaving behind open, interconnected microchannels that provide the desired embedded vascular networks.

Endothelialization of Vascular Networks: The embedded vascular networks were flushed with ca. 500 μL of EGM-2 cell media and then injected with ca. 5–10 μL of HUVEC suspensions (1×10^7 cells mL^{-1}). The structures were inverted and incubated at 37 °C for 30 min. After 30 min, the entire structure was flipped and again incubated at 37 °C for 30 min to ensure that the top and bottom of the channels were exposed to HUVECs. The structures were then incubated at 37 °C for 5 h, after which they were placed on a rocker oscillating at ca. 1 Hz frequency within the incubator. After 24 h, non-adherent cells were flushed out of the network with fresh EGM-2 media and the construct was placed back on the rocker at ca. 1 Hz frequency. For improved cell adhesion, the channels could be coated with fibronectin (BD Technologies) solution (0.010 mg mL^{-1}) for 30 min prior to introducing the HUVEC suspension.

Cell Viability Assay: Cell viability was determined by printing a cell-laden GelMA ink composed of 2×10^6 cells mL^{-1} 10 T1/2 fibroblasts and HNDFs. Four printed structures were fabricated for each time point. The samples were prepared by staining with calcein-AM ("live", 1 μL mL^{-1}, Invitrogen) and ethidium homodimer ("dead", 4 μL mL^{-1}, Invitrogen) for 20 min. Control samples are produced by casting cell-laden GelMA films (200–300μm thick) composed of the same cell type, density, and GelMA composition, and exposed to the same curing process, as the printed samples. Data were acquired using confocal microscopy for each time point (t = 0,1,3,5,7 days, n = 10), and average viability and standard deviations were determined for each sample. A student's t-test was used to compare the viability of printed versus control cell populations. Differences with p values less than 0.05 are denoted with asterisks.

Imaging and Image Analysis: Photographs and videos of the 3D printed, engineered tissue constructs were captured using a DSLR camera (Canon EOS 5D Mark II, Canon U.S.A Inc.). To aid in visualizing the embedded vascular networks, an aqueous based-fluorescent red dye (Risk Reactor) was directly injected into the network using a syringe. Microscopy was performed using a Keyence zoom microscope (VHX-2000, Keyence, Japan), an inverted fluorescence microscope (Axiovert 40 CFL, Zeiss), an upright confocal microscope (LSM710, Zeiss), and an upright fluorescent microscope (Axiozoom V16, Zeiss). Composite microscopy images were generated using ImageJ by combining bright field and fluorescent channels. 3D projections and *Z*-stacks were generated using manual and automated processes in Imaris (Imaris 7.6.4, Bitplane Scientific Software) and ImageJ software. For cell counting, a semiautomated counting algorithm in Imaris was used to produce counting statistics. For extended microscopy experiments, samples were first fixed using 4% paraformaldehyde solution (Electron Microscopy Sciences), stained with DAPI nuclear stain (Life Technologies) and kept hydrated using DPBS with 0.05% Tween-20 (Sigma)

Supporting Information

Supporting Information is available from the Wiley Online Library or from the author.

Acknowledgements

The authors thank the Wyss Institute for Biologically Inspired Engineering and the Harvard MRSEC (NSF DMR 0820484) for their generous support of this research. R.L.T. is supported in part by a National Science Foundation Graduate Research Fellowship Program under Grant No. DGE1144152. The authors also thank Dr. Yevgeny Brudno and Prof. David Mooney for generously donating cell lines and for useful discussions and Thomas Ferrante and Wyss core imaging facilities for their assistance. Finally, the authors thank several members of thei group, Dr. Mark Scott, Dr. Brett Compton, Dr. James Hardin IV, and Dr. Scott Slimmer, for helpful discussions, and Valentina Lyau and Chun-Wei (Leo) Chang for their experimental assistance.

Received: November 5, 2013
Revised: December 21, 2013
Published online: February 18, 2014

[1] R. Langer, J. Vacanti, *Science* **1993**, *260*, 920.
[2] K. Bhadriraju, C. S. Chen, *Drug Discovery Today* **2002**, *7*, 612.
[3] A. Atala, F. K. Kasper, A. G. Mikos, *Sci. Transl. Med.* **2012**, *4*, 160rv12.
[4] V. Mironov, T. Boland, T. Trusk, G. Forgacs, R. R. Markwald, *Trends Biotechnol.* **2003**, *21*, 157.
[5] V. Mironov, R. P. Visconti, V. Kasyanov, G. Forgacs, C. J. Drake, R. R. Markwald, *Biomaterials* **2009**, *30*, 2164.
[6] C. Zandonella, *Nature* **2003**.
[7] M. Radisic, L. Yang, J. Boublik, R. J. Cohen, R. Langer, L. E. Freed, G. Vunjak-Novakovic, *Am. J. Physiol. Heart Circ. Physiol.* **2004**, *286*, H507.
[8] C. K. Griffith, C. Miller, R. Sainson, J. W. Calvert, N. L. Jeon, C. W. Hughes, S. C. George, *Tissue Eng.* **2005**, *11*, 257.
[9] H. Lodish, B. Arnold, P. Matsudaira, C. Kaiser, M. Krieger, M. Scott, S. L. Zipursky, J. Darnell, Molecular Cell Biology, W. H Freeman and Company, New York, **2000**.
[10] B. Derby, *Science* **2012**, *338*, 921.
[11] S. J. Hollister, *Nat. Mater.* **2005**, *5*, 518.
[12] D. W. Hutmacher, *Biomaterials* **2000**, *21*, 2529.
[13] A. J. Reiffel, C. Kafka, K. A. Hernandez, S. Popa, J. L. Perez, S. Zhou, S. Pramanik, B. N. Brown, W. S. Ryu, L. J. Bonassar, J. A. Spector, *PLoS ONE* **2013**, *8*, e56506.
[14] D. L. Cohen, E. Malone, H. Lipson, L. J. Bonassar, *Tissue Eng.* **2006**, *12*, 1325.
[15] M. S. Mannoor, Z. Jiang, T. James, Y. L. Kong, K. A. Malatesta, W. O. Soboyejo, N. Verma, D. H. Gracias, M. C. McAlpine, *Nano Lett.* **2013**, *13*, 2634.
[16] C. Norotte, F. S. Marga, L. E. Niklason, G. Forgacs, *Biomaterials* **2009**, *30*, 5910.
[17] J. S. Miller, K. R. Stevens, M. T. Yang, B. M. Baker, D.-H. T. Nguyen, D. M. Cohen, E. Toro, A. A. Chen, P. A. Galie, X. Yu, R. Chaturvedi, S. N. Bhatia, C. S. Chen, *Nat. Mater.* **2012**, *11*, 768.
[18] D. Therriault, S. R. White, J. A. Lewis, *Nat. Mater.* **2003**, *2*, 265.
[19] W. Wu, A. DeConinck, J. A. Lewis, *Adv. Mater.* **2011**, *23*, H178.
[20] M. Bohorquez, C. Koch, T. Trygstad, N. Pandit, *J. Colloid Interface Sci.* **1999**, *216*, 34.
[21] S. Sharma, K. Tantisira, V. Carey, A. J. Murphy, J. Lasky-Su, J. C. Celedón, R. Lazarus, B. Klanderman, A. Rogers, M. Soto-Quirós, L. Avila, T. Mariani, R. Gaedigk, S. Leeder, J. Torday, D. Warburton, B. Raby, S. T. Weiss, *Am. J. Respir. Crit Care Med.* **2010**, *181*, 328.
[22] J. W. Nichol, S. T. Koshy, H. Bae, C. M. Hwang, S. Yamanlar, A. Khademhosseini, *Biomaterials* **2010**, *31*, 5536.
[23] V. Normand, S. Muller, J.-C. Ravey, A. Parker, *Macromolecules* **2000**, *33*, 1063.
[24] A. I. Van Den Bulcke, B. Bogdanov, N. De Rooze, E. H. Schacht, M. Cornelissen, Berk, *Biomacromolecules* **2000**, *1*, 31.
[25] M. Nikkhah, N. Eshak, P. Zorlutuna, N. Annabi, M. Castello, K. Kim, A. Dolatshahi-Pirouz, F. Edalat, H. Bae, Y. Yang, A. Khademhosseini, *Biomaterials* **2012**, *33*, 9009.
[26] A. Krogh, *J. Physiol.* **1919**, *52*, 409.
[27] C. Michiels, *J. Cell. Physiol.* **2003**, *196*, 430.
[28] Q. Shen, *Science* **2004**, *304*, 1338.
[29] J. M. Butler, H. Kobayashi, S. Rafii, *Nat Rev Cancer* **2010**, *10*, 138.
[30] D.-H. T. Nguyen, S. C. Stapleton, M. T. Yang, S. S. Cha, C. K. Choi, P. A. Galie, C. S. Chen, *Proc. Natl. Acad. Sci. USA* **2013**, *110*, 6712.
[31] Y. Zheng, J. Chen, M. Craven, N. W. Choi, S. Totorica, A. Diaz-Santana, P. Kermani, B. Hempstead, C. Fischbach-Teschl, J. A. López, A. D. Stroock, *Proc. Natl. Acad. Sci. USA* **2012**, *109*, 9342.
[32] B. A. Aguado, W. Mulyasasmita, J. Su, K. J. Lampe, S. C. Heilshorn, *Tissue Eng., A* **2012**, *18*, 806.
[33] R. Chang, J. Nam, W. Sun, *Tissue Eng., A* **2008**, *14*, 41.
[34] C. M. Smith, J. J. Christian, W. L. Warren, S. K. Williams, *Tissue Eng.* **2007**, *13*, 373.
[35] C. J. Hansen, R. Saksena, D. B. Kolesky, J. J. Vericella, S. J. Kranz, G. Muldowney, K. T. Christensen, J. A. Lewis, *Adv. Mater.* **2013**, *25*, 96.